

## Article

# Magnetic Nanosorbents Based on Bentonite and $\text{CoFe}_2\text{O}_4$ Spinel

Nataliya Khodosova <sup>1</sup>, Lyudmila Novikova <sup>1,\*</sup> , Elena Tomina <sup>1,2</sup>, Larisa Belchinskaya <sup>1</sup>, Alexander Zhabin <sup>2</sup>, Nikolay Kurkin <sup>2</sup> , Victoria Krupskaya <sup>3</sup> , Olga Zakusina <sup>3</sup>, Tatiana Koroleva <sup>3,4</sup>, Ekaterina Tyupina <sup>5,6</sup> , Alexander Vasiliev <sup>7</sup> and Pavel Kazin <sup>7</sup> 

<sup>1</sup> Department of Chemistry, Voronezh State University of Forestry and Technologies Named after G.F. Morozov, 8 Timiryazeva Str., 394087 Voronezh, Russia

<sup>2</sup> Department of General Geology and Geodynamics, Voronezh State University, 1 Universitetskaya pl., 396036 Voronezh, Russia

<sup>3</sup> Institute of Geology of Ore Deposits, Petrography, Mineralogy and Geochemistry RAS, 35, Staromonetny per., 119017 Moscow, Russia

<sup>4</sup> Faculty of Geology, M.V. Lomonosov Moscow State University, GSP-1, Leninskie Gory, 119991 Moscow, Russia

<sup>5</sup> Department of High Energy Chemistry and Radioecology, Mendeleev University of Chemical Technology of Russia, 9, Miusskaya Square, 125047 Moscow, Russia

<sup>6</sup> Department of Closed Nuclear Fuel Cycle Technology, National Research Nuclear University MEPhI, Kashirskoe Highway 31, 115409 Moscow, Russia

<sup>7</sup> Department of Chemistry, M.V. Lomonosov Moscow State University, 119991 Moscow, Russia

\* Correspondence: yonk@mail.ru; Tel.: +7-(473)-2537-659

**Abstract:** New magnetic nanocomposite sorbents were obtained by doping natural bentonite with nanosized  $\text{CoFe}_2\text{O}_4$  spinel (10 and 20 wt.%). Nanocrystals of cobalt ferrite were synthesized by a citrate burning method. The structure and physical-chemical properties of the composites were characterized by XRD, XRF, TEM, BET, FTIR and Faraday balance magnetometry. During the formation of nanocomposites, 10–30 nm particles of cobalt ferrite occupied mainly the interparticle space of Fe-aluminosilicate that significantly changed the particle morphology and composite porosity, but at the same time retained the structure of the 2:1 smectite layer. A combination of two functional properties of composites, adsorption and magnetism has been found. The adsorption capacity of magnetic nanosorbents exceeded this parameter for bentonite and spinel. Despite the decrease in the adsorption volume, pore size and specific surface area of the composite material relative to bentonite, the sorption activity of the composite increases by 12%, which indicated the influence of the magnetic component on the sorption process. FTIR data confirmed the mechanism of formaldehyde sorption by the composite sorbent. The production of a magnetic nanosorbent opens up new possibilities for controlling the sorption processes and makes it possible to selectively separate the sorbent from the adsorption medium by the action of a magnetic field.

**Keywords:** nanocomposite; bentonite; smectite; cobalt ferrite; citrate synthesis; sorption; formaldehyde; magnetically controlled sorbent



**Citation:** Khodosova, N.; Novikova, L.; Tomina, E.; Belchinskaya, L.; Zhabin, A.; Kurkin, N.; Krupskaya, V.; Zakusina, O.; Koroleva, T.; Tyupina, E.; et al. Magnetic Nanosorbents Based on Bentonite and  $\text{CoFe}_2\text{O}_4$  Spinel. *Minerals* **2022**, *12*, 1474. <https://doi.org/10.3390/min12111474>

Academic Editor: Martin P. Pentrak

Received: 26 October 2022

Accepted: 19 November 2022

Published: 21 November 2022

**Publisher's Note:** MDPI stays neutral with regard to jurisdictional claims in published maps and institutional affiliations.



**Copyright:** © 2022 by the authors. Licensee MDPI, Basel, Switzerland. This article is an open access article distributed under the terms and conditions of the Creative Commons Attribution (CC BY) license (<https://creativecommons.org/licenses/by/4.0/>).

## 1. Introduction

Adsorption technology for the purification and separation of substances is an integral part of most modern industries [1–6]. Due to the easy construction and operating of adsorption filters and systems, reproducibility of their characteristics, efficiency and economy of the process as a whole, the use of adsorption technology is one of the most affordable ways to treat wastewaters and emissions at enterprises. Among the variety of synthetic (polymer resins [7], silicon oxide [8], etc.) and natural (activated carbon, zeolites, clays, etc. [9–11]) sorption materials, the latter are more demanded as available and low-cost ones, with a possibility of targeted modification [12–14], as well as the environmental friendliness of their production.

However, both natural and synthetic sorbents are not without drawbacks associated with their regeneration, loss of sorption capacity, disposal and, often, the impossibility of easy separation from the liquid phase that is especially hard in case of finely dispersed sorbents, such as clay minerals. The solution of one of these problems became possible with the advent of the synthesis methods for magnetically sensitive and magnetically controlled composite materials, the development and application of which has marked by the great interest in recent research [15–18]. By incorporating the small amounts of nanosized magnetic materials into the composite matrix it is possible, without a significant rise of its cost, to render its saturation magnetization sufficient for its easy separation from the liquid phase applying an external magnetic field and, thereby, significantly simplify, intensify and improve the efficiency of sorption technology for the purification of substances [1,19–22].

Most often, for the synthesis of magnetic composite materials, nanoparticles of iron oxide have been used as the main components [15,23–26]. Nanosized magnetic sorbents manifest their high potential in eliminating both heavy metal ions, such as arsenic, lead, mercury [27–29] and organic pollutants (dyes, antibiotics) [30–32] from wastewaters due to the ultrafine state and high selectivity in the absorption of toxicants [33,34]. In addition to iron oxides, nanosized metal ferrites with a spinel structure ( $\text{MeFe}_2\text{O}_4$ , where Me = Zn, Ni, Mg, Co, Mn) have been successfully used for the synthesis of sorbents with magnetic properties. They reveal chemical resistance in acidic media, thermal stability, a well-developed surface and high saturation magnetization [35–40]. Among the known ferrites, cobalt ferrite  $\text{CoFe}_2\text{O}_4$  seems to be promising, as it is capable of a fast super-paramagnet/ferromagnet transition [41]. High coercive force of cobalt ferrite  $\text{CoFe}_2\text{O}_4$ , which is a ferromagnet with a Curie temperature of 793 K [42,43], allows one to use cobalt spinel and its composite materials as magnetic sorbents that can be easily removed from an aqueous suspension under the action of a magnetic field from a permanent magnet [36,37].

It is known that the physical and chemical properties of nanosized materials largely depend on the way of its preparation, which determines the crystallinity, morphology, size of particles and the presence of impurities. The combination of cobalt ferrite properties with those of the other materials, such as a developed specific surface area, a presence of micro- and mesoporosity, as well as active surface sites of various natures, is perspective for developing a new composite magnetically controllable sorbent. Among such materials, natural aluminosilicates have been extensively used, owing to their structure and morphology variety, in addition to their rich deposits available. Particularly, microporosity of natural zeolite faujasite was efficiently used in [1] for the synthesis of the  $\text{CoFe}_2\text{O}_4$ -composite ion-exchange material with an enhanced sorption capacity to  $\text{Pb}^{2+}$ -ions (purification rate ~99%). Layered minerals [44,45], LDH [46] and other layered materials can incorporate nanoparticles of ferrites within the interparticle space that raised significantly (by 40%–60%) the sorption rate of bulky organic molecules [45,46] and was able to change their properties so dramatically that magnetic particles became hydrophilic, stable, bioavailable and biocompatible [18]. However, as found in [35], the addition of nanosized cobalt ferrite to the natural layered mineral vermiculite in order to form a magnetically active composite sorbent resulted in a twofold decrease of the specific surface area of the sorbent and a subsequent decline of its sorption capacity for methylene blue by 28%–52%.

Recently, a pilot study was done in [47] to assess the possibility of using natural clay mineral nontronite, a layered ferruginous aluminosilicate from the smectite group, for developing the new sorption composite material with a predictable magnetic sensitivity. The introduction of 20 wt.% of  $\text{CoFe}_2\text{O}_4$  spinel into the composite compound did not decrease its sorption capacity regarding the industrial toxicant formaldehyde as compared to natural aluminosilicate, but, on the contrary, slightly raised it. This fact agrees with the aforesaid works [44–46], though it contradicts the findings of [35], indicating a decrease in the sorption capacity of minerals upon modification with ferrites. It should be noted that the effect of the Fe-smectite modification with cobalt ferrite [47] was weaker than that of a common acid modification, reaching a 2.6-times increase in the sorption capacity of Fe-smectite towards formaldehyde. However, the emergence of magnetic susceptibility

in the new sorbent material was expected as its indisputable advantage, along with the environmentally benign way of its production, of generating no effluents, as compared to the reagent activation of clay.

Considering the contradictory and insufficient evidences on the rise or decrease in the sorption capacity of aluminosilicate/cobalt ferrite composites available in the literature, as well as the prospects for the practical application of magnetically sensitive sorption material in the area of industrial wastewater treatment technology, the goal of this work was set to form the nanostructured composites with adsorption and magnetic functional properties on the base of natural Fe-aluminosilicate doped with the synthesized nanodispersed spinel of  $\text{CoFe}_2\text{O}_4$ .

## 2. Materials and Methods

For the synthesis of new composite sorbents, a sample of clay material (Bt) rich in the content of natural layered aluminosilicate of the smectite group (Buturlinskoye deposit, Voronezh region, Russia) and synthesized samples of cobalt ferrite  $\text{CoFe}_2\text{O}_4$  (F) were used. The Buturlinskoye deposit has a sedimentary genesis and belongs to the Kiev horizon of the Upper Eocene [48]. The deposit has not been exploited recently. Up until the 1990s, raw materials were used for keramzite (expanded clay) production. Samples for the study were collected from the walls of the quarry. They were crushed and sieved into 200–315  $\mu\text{m}$  fraction and not subjected to any additional treatments described in the manuscript.

### 2.1. Synthesis of Cobalt Ferrite $\text{CoFe}_2\text{O}_4$

The sample of cobalt ferrite (F) was synthesized by a citrate combustion method [49–51]. The citrate combustion method is technically simple and convenient for obtaining highly dispersed oxide materials, as it involves a complexing agent for the intermediate polymer gel synthesis, which is then burned out. As a result, it is possible to synthesize monophasic nanopowders with a homogeneous microstructure, at lower temperatures and shorter reaction times as compared to traditional sintering methods.

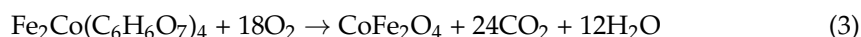
For the synthesis of the  $\text{CoFe}_2\text{O}_4$  spinel, stoichiometric quantities of crystal hydrates of iron (III) nitrate (analytical grade, TU 6-09-02-553-96, JSC “Ural Plant of Chemical Reagents”, Russia) and cobalt (II) nitrate (analytical grade, CAS 10035-06-0, LLC “Spectr-Khim”, Russia) were dissolved in distilled water. Then, 28% of an ammonia solution (chemically purity grade, GOST 3760-79, JSC “LenReaktiv”, Russia) was added in the amount required to form hydroxides of cobalt (II) and iron (III) according to the chemical equation below, avoiding an excess of  $\text{NH}_4\text{OH}$  and the formation of ammonia complexes:



Further, to dissolve a mixture of the  $\text{Fe}(\text{OH})_3$  and  $\text{Co}(\text{OH})_2$  formed, a portion of 1 M citric acid solution was added under mild heating. The resulting solution of iron-cobalt citrate was evaporated until a dark red gel formed:



Upon further heating, the gel ignited with the formation of a black powder of  $\text{CoFe}_2\text{O}_4$ , according to the stoichiometric equation:



The obtained powder of  $\text{CoFe}_2\text{O}_4$  was washed with distilled water, filtered, air-dried and annealed in the muffle furnace (SNOL 8.2/1100) at 600 °C for 1 h to remove water and residues of organic substances.

## 2.2. Fabrication of Nanocomposites

The samples of nanocomposites (Bt-10F and Bt-20F) were obtained according to the procedure suggested earlier in [47]. For this, portions of 10/20 mass % of cobalt ferrite and 80/90 mass % of natural clay material were thoroughly mixed in a small amount of ethanol to form a paste. The resulted paste was air-dried and annealed in the muffle oven (SNOL 8.2/1100) at 500 °C for 1 h.

## 2.3. Methods for Composition Diagnostics

The chemical composition of the samples Bt, Bt-10F and Bt-20F was derived from the XRF data obtained using the S8 Tiger spectrometer (Bruker AXS GmbH, Karlsruhe, Germany) following standard procedure. Prior to the analysis, samples were crushed to a fraction size of 50 µm, dried at 110 °C and fused with lithium tetraborate at 1150 °C for 10 min. The results were treated using the SpectraPlus software (Bruker AXS GmbH, Germany).

The X-ray diffraction analysis was performed using an Ultima-IV X-ray diffractometer (Rigaku, Tokyo, Japan). The diffractometer configuration consisted of: Cu-K $\alpha$  radiation, D/Tex-Ultra detector, scan range 3–65° 2 $\theta$ , fixed focusing slit system. The study of the sample composition was carried out using non-oriented preparations, which provides maximal disorientation of the particles necessary to obtain high-quality diffraction patterns for calculating the quantitative mineral composition. The mineral composition was diagnosed by comparing the experimental and reference (from the PDF-2 database [52]) diffraction patterns using the Jade 6.5 software package (MDI company, Newtown Square, PA, USA).

The FTIR-spectroscopic studies were done by applying the FTIR-spectrometer Vertex-70 (BrukerOptik GmbH, Ettlingen, Germany) equipped with the Platinum ATR accessory with a diamond crystal, at the Center for the Collective Use of Scientific Equipment of the Voronezh State University. The spectra were recorded in the mode of attenuated total reflectance with 256 scans for each sample in the range of a 4000–400 cm<sup>-1</sup> and 0.4 cm<sup>-1</sup> resolution. The results were treated in the Opus 8.0 software.

For the additional characterization of the main mineral bentonite (smectite), its KBr preparation was studied on a Perkin Elmer Spectrum One FT-IR spectrometer equipped with an indium gallium arsenide (InGaAs) detector and a KBr beam splitter to study the fine structure of natural aluminosilicate. The IR spectrum was measured in the range of 4000–400 cm<sup>-1</sup>. For the measurement, a tablet was made by pressing the 0.5 mg of the sample and 200 mg of KBr for 20–25 min. The spectra were processed using the OPUS 7.2 software package (Bruker Ltd., Billerica, MA, USA). The baseline correction was performed interactively by a linear method with one iteration.

## 2.4. Methods for the Properties Analysis

The particle size and morphology of Bt, CoFe<sub>2</sub>O<sub>4</sub> and composites based on them were characterized from the TEM-images taken at the Carl Zeiss Libra-120 electronic microscope. A quantitative elemental analysis of a CoFe<sub>2</sub>O<sub>4</sub> spinel sample was carried out using a JSM-6380LV JEOL scanning electron microscope with an INCA 250 microanalysis system at an accelerating voltage of 20 kV (resolution of up to 3 nm in a high vacuum mode, elements range from boron to plutonium).

The values of the specific surface area of the samples were assessed by the experimental nitrogen sorption-desorption isotherms at –196 °C using the QuadraSorb Quantachrome Instruments unit (Boynton Beach, FL, USA). The samples (150 mg) were outgassed at 100 °C for 4 h. The values of total pore volume and average pore diameter were calculated by the DFT method with the Quantachrome QuadraWin Software (version 5.1, Quantachrome Instruments unit, Boynton Beach, FL, USA).

The sorption capacity of the investigated samples of natural bentonite, CoFe<sub>2</sub>O<sub>4</sub> and composites Bt-10F and Bt-20F was assessed towards formaldehyde in aqueous solutions, which is a toxic aldehyde of the 2nd hazard class [53]. Isotherms of formaldehyde adsorption from aqueous solutions in the concentration range of 0.038–0.38 M were studied.

To determine the adsorption capacity, 0.5 g of a sorbent was placed in a flask filled with 0.025 dm<sup>3</sup> of the formaldehyde solution of specified concentration, covered with a lid, shaken and left for 2 h at 20 °C to reach sorption equilibrium. Afterwards, the equilibrium solution was filtered through a paper filter and the equilibrium concentration of the formaldehyde was determined using a sulfite method. The relative error of determination was 1%–3%.

The magnetic susceptibility of the samples and their ability of magnetic separation was qualitatively assessed using a 30 × 10 mm in size neodymium magnet, N42 (China) (residual magnetic induction 1.30–1.33 T, coercive force 12 kOe). The magnet was attached to the flask with the sorbent and the equilibrium solution, and the ability of the suspension for separation under a magnetic field was watched.

Quantitatively, magnetic properties of the investigated samples were characterized by measuring the magnetization curves using the Faraday balance (manufactured at the Institute of Solid State Chemistry of the Ural branch of the Russian Academy of Sciences) at room temperature. The magnetic field was varied from −17.9 to 17.9 kOe. The relative error in determining the magnetization was 3%. The error in determining the coercive force was ±100 Oe.

### 3. Results and Discussion

#### 3.1. Characterization of Composition and Structure of CoFe<sub>2</sub>O<sub>4</sub>, Natural Aluminosilicate and Composites on Their Base

As follows from the X-ray phase analysis (Figures 1 and S1), the sample of cobalt ferrite synthesized is fully monophasic [45]. The set of reflections in the diffraction pattern corresponds to the cobalt ferrosilicate CoFe<sub>2</sub>O<sub>4</sub> (PDF#22-1086). According to the data of the local X-ray spectral microanalysis, the real chemical composition of the synthesized cobalt ferrite is represented by the elements (at %): Co (14.44); Fe (28.73); and O (56.83), which can be expressed by the following chemical formula: Co<sub>1.005</sub>Fe<sub>2</sub>O<sub>3.95</sub>.

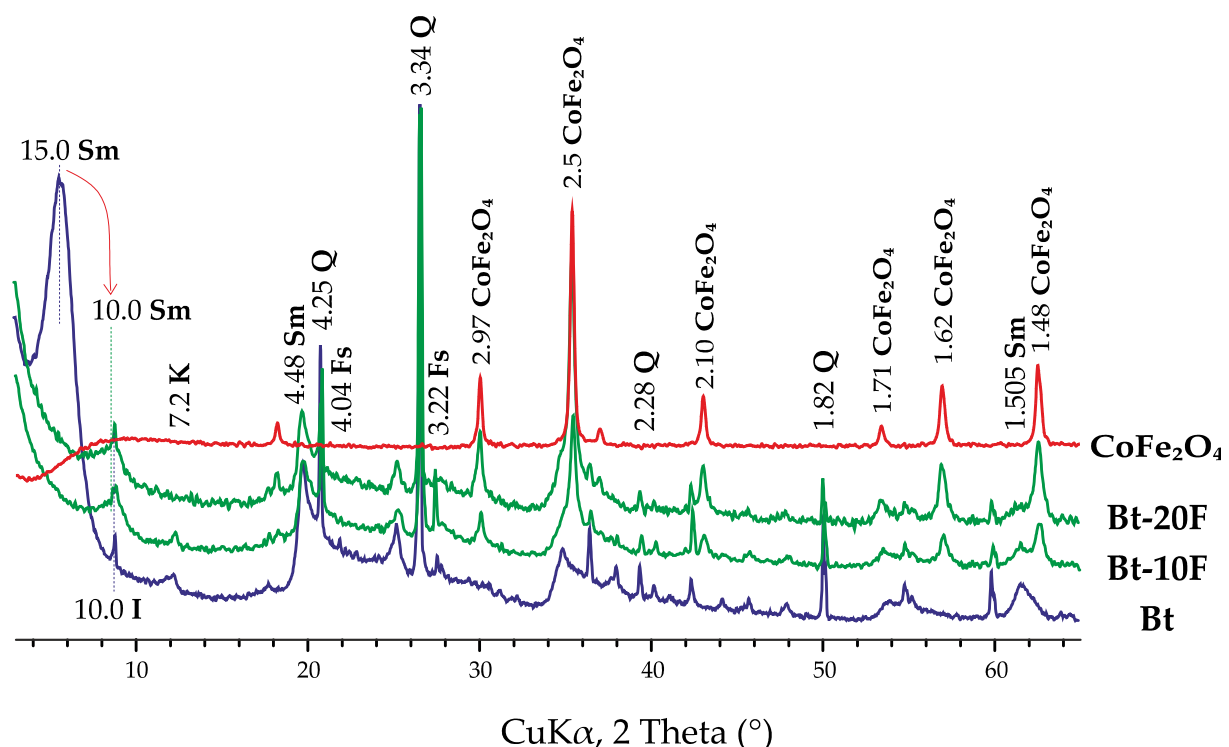


**Figure 1.** XRD patterns of investigated samples of Bt, CoFe<sub>2</sub>O<sub>4</sub> and composites Bt-10F, Bt-20F. Phase designations: Sm—smectite, I—illite, K—kaolinite, Q—quartz, Fs—feldspars.

The sample of the natural clay material taken for investigation was represented mainly by the aluminosilicate of the smectite group (66.6%) with a slight admixture of other clay (kaolinite 5.5% and illite 5.2%) and non-clay (quartz 8.9%, feldspars 11.8%, anatase 1.5% and calcite 0.5%) minerals. The value of the interplanar distance of the reflection (060)—1.503 Å testified to dioctahedral smectite. The position of the (001) reflection with  $d = 15.0$  Å allows one to deduce the predominant content of Ca and Mg cations in the interlayer of smectite. Other clay minerals were represented by illite (with a series of basal reflections  $d = 9.9, 5.0$  Å, etc.) and kaolinite (with a series of basal reflections  $d = 7.18$  Å, etc.). Non-clay minerals were represented by quartz ( $d = 4.25, 3.34, 2.46, 2.28, 2.13, 1.82, 1.54$  Å, etc.), calcite (with a small reflection  $d = 3.03$  Å), feldspars albite and microcline (with low-intensity reflections  $d = 4.04, 3.22, 3.19$  Å, etc.) and anatase ( $d = 3.52, 2.37$  Å, etc.).

In the FTIR-spectra of bentonite (Figure 2a,b) it is clearly seen that its main component is dioctahedral smectite, while impurities include kaolinite and quartz. There are two characteristic ranges of vibrations for dioctahedral smectite:  $3800\text{--}3200\text{ cm}^{-1}$  and  $1600\text{--}400\text{ cm}^{-1}$ . Although the admixture of kaolinite (bands at  $3695, 3621$  and  $695\text{ cm}^{-1}$ ) makes it impossible to diagnose the band of stretching vibrations of smectite OH-groups and the IR spectra in the region of  $1600\text{--}400\text{ cm}^{-1}$  is characteristic of Fe-smectite [54]. The band at  $1038\text{ cm}^{-1}$  is assigned to stretching vibrations of Si-O, and bands at  $918\text{ cm}^{-1}$  and  $882\text{ cm}^{-1}$  are due to the bending vibrations of Al-Al-OH and Al-Fe<sup>3+</sup>-OH, respectively; bands at  $470\text{ cm}^{-1}$  and  $526\text{ cm}^{-1}$  are assigned to the deformation vibrations of Si-O-Si and Al O-Si, correspondingly [9,55,56]. The bands at  $797$  and  $780\text{ cm}^{-1}$  are related to the quartz impurity. Despite the fact that the name “Fe-smectite” for the predominant phase can be considered as more general, this phase cannot be attributed to nontronite, as we indicated earlier [14,47].

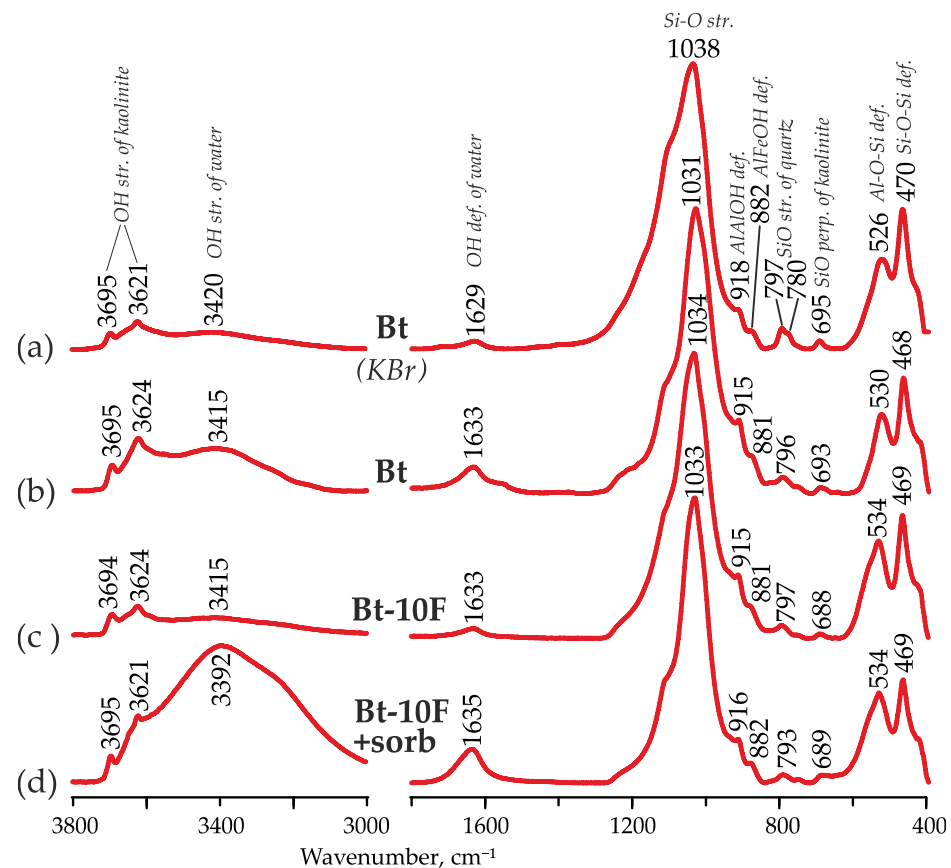


**Figure 2.** FTIR-spectra of investigated samples of bentonite (a,b), composite Bt-10F (c) and composite after adsorption of formaldehyde—Bt-10F + sorb (d).

As the samples Bt-10F and Bt-20F (Figure 1) are the composite fabricated from the samples of the natural clay material and synthetic  $\text{CoFe}_2\text{O}_4$ , their diffraction patterns show reflections from the phases of both samples with various quantitative ratios. A distinguishing feature of composites was a decrease in the interplanar distance of the (001) smectite reflection to 10 Å, which, along with the presence of all other non-basal reflections, indicated the preservation of the 2:1 structure of the smectite layer and, at the same time, significant dehydration of the interlayer space.

The addition of 10 mass % of  $\text{CoFe}_2\text{O}_4$  into the composite material practically did not change the FTIR-spectrum of clay material (Figure 2c). The presence of distinctive absorption bands of stretching vibrations of the octahedral Co-O and tetrahedral Fe-O group complexes [17,57] of cobalt ferrite near  $685\text{ cm}^{-1}$  and  $411\text{ cm}^{-1}$  was not observed in the spectrum of composite, obviously, due to their low intensity and overlapping with bands of Si-O-Si [56] in this spectral region.

Chemical compositions of the natural clay material and composites on its base are summarized in Table 1 and Table S1 of Supplementary Materials.

**Table 1.** Chemical compositions of clay material and composites samples.

Sample	Oxide Content, Mass %									LOI	Total
	SiO <sub>2</sub>	Al <sub>2</sub> O <sub>3</sub>	MgO	K <sub>2</sub> O	CaO	TiO <sub>2</sub>	Fe <sub>2</sub> O <sub>3</sub>	Na <sub>2</sub> O	CoO		
Bt	67.67	12.55	1.22	1.04	2.01	4.21	10.33	0.10	n.d.	6.57	99.80
Bt-10F	53.90	11.85	1.35	0.83	1.48	3.05	18.04	0.11	4.70	4.52	99.92
Bt-20F	44.94	9.27	1.21	0.66	1.56	2.74	24.49	0.17	8.33	6.45	99.91

The addition of spinel to the clay material caused a regular decrease in the content of oxides  $\text{Al}_2\text{O}_3$ ,  $\text{SiO}_2$ ,  $\text{CaO}$ ,  $\text{TiO}_2$ ,  $\text{K}_2\text{O}$  and  $\text{MgO}$  and an increase in the content of  $\text{Fe}_2\text{O}_3$  and  $\text{CoO}$ .

TEM data in Figure 3a,b illustrated the irregular shape of cobalt ferrite particles with a tendency to apparent agglomeration. The size of the particles ranged from 20 to 120 nm with a predominance of 40–80 nm-sized fraction.

As follows from the TEM data, rod-shaped particles of Fe-smectite were elongated in one direction having a length of 100–300 nm and a width of up to 50 nm, with a significant degree of agglomeration (Figure 3c). At the same time, the images illustrated the appearance of round semitransparent particles with a size of about 20 nm. The varying morphology of the particles was probably caused by mechanical influences during the samples' preparation for analytical studies.

The sample of nanocomposite Bt-20F, synthesized as a mechanical mixture of ready-made precursors, represented an irregular shape of particles of aluminosilicate of 10–50 nm (light-gray rounded formations, Figure 3d), with inclusions of individual particles of cobalt ferrite of 10–30 nm (few dark particles, Figure 3d). The TEM-image of Bt-20F sample clearly testified that the elongated rod-like shape of particles of original bentonite disappeared, which was apparently associated with the changes in the pore space and the character of aluminosilicate particles' interactions caused by annealing of the nanocomposite. Based on the previously published data for the samples from the deposit close in location and genesis, the dehydroxylation temperature of a Fe-smectite sample is  $490\text{ °C}$  [58]. However, the obtained X-ray diffraction characteristics of the composites (Figure 1), as well as the preservation of reflections of kaolinite, which is less resistant to heat than smectites, evidenced that a 1 h exposure of composites to high temperatures by annealing did not lead to the significant changes in the structure of the smectite layer.

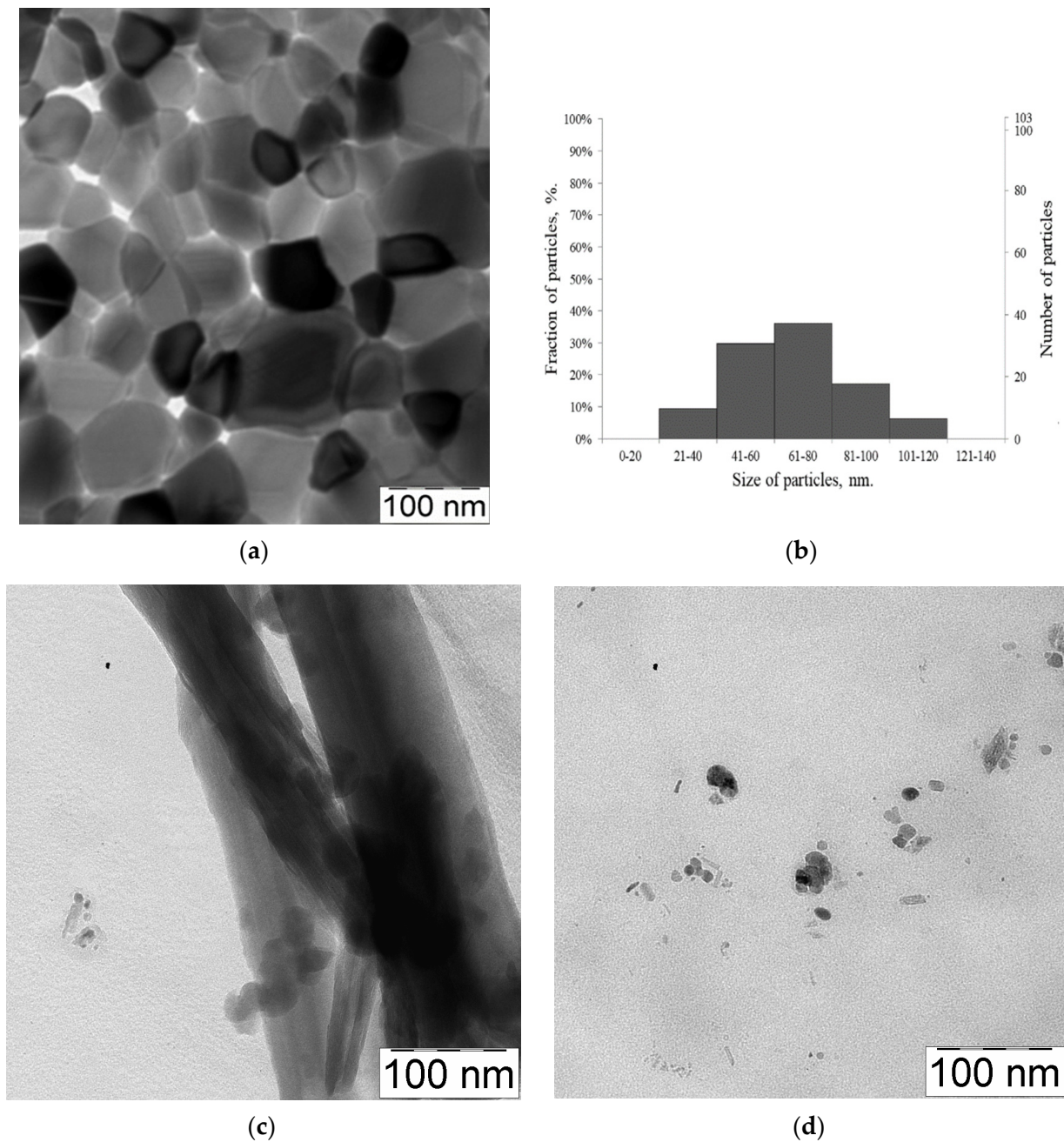


**Figure 3.** TEM images of investigated samples: (a) CoFe<sub>2</sub>O<sub>4</sub>; (b) particle size distribution of CoFe<sub>2</sub>O<sub>4</sub>; (c) Fe-smectite; (d) nanocomposite Bt-20F.

### 3.2. Characterization of the Sorption Ability of Ferrite, Fe-Smectite and Composites on Their Base

Figure 4a represents isotherms of N<sub>2</sub> sorption-desorption by the investigated samples of Bt, CoFe<sub>2</sub>O<sub>4</sub> and the composite on their base.

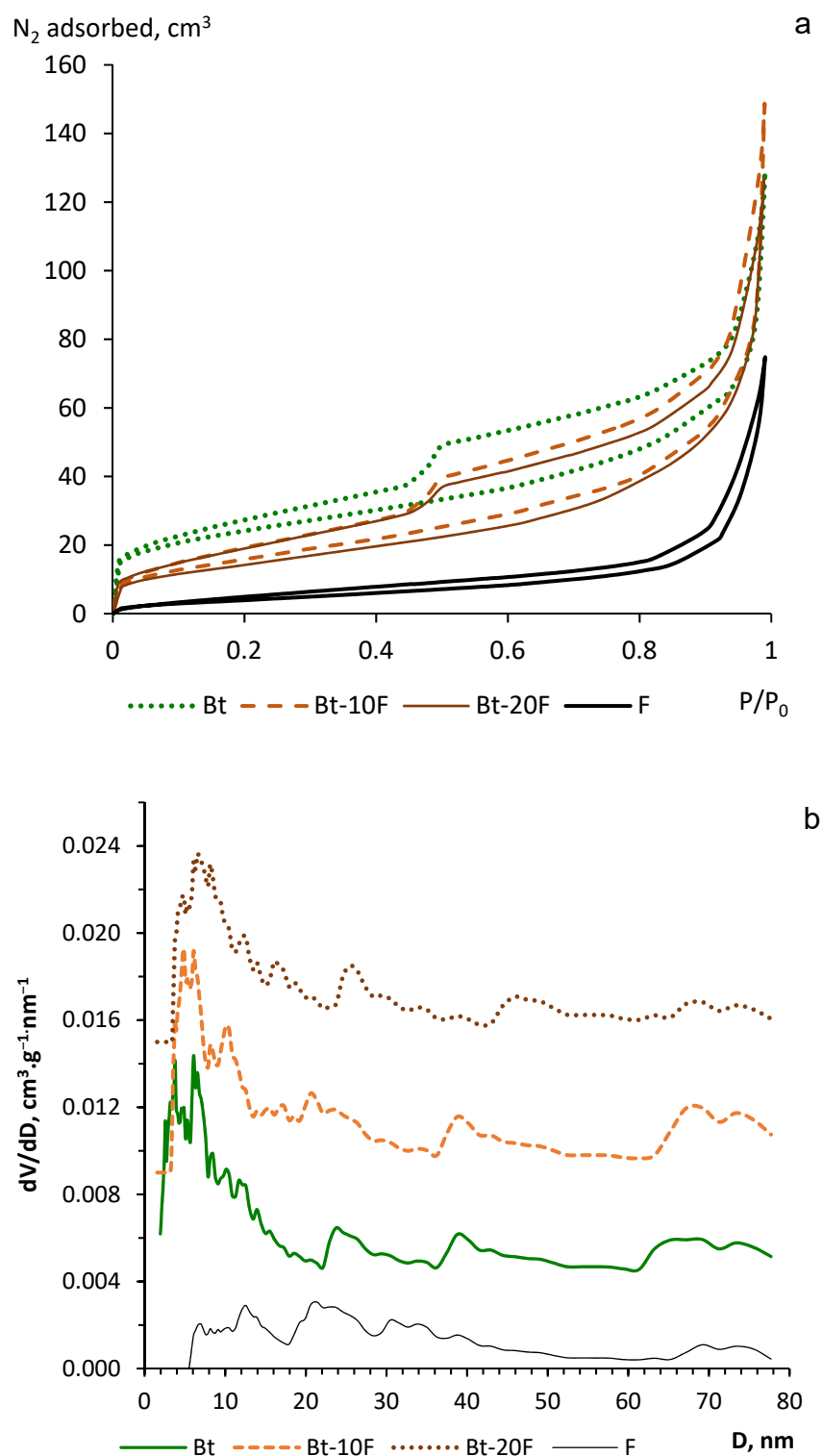


**Figure 4.** Isotherms of N<sub>2</sub> adsorption-desorption (a) and pore size distribution (b) for samples of Bt, Bt-10F, Bt-20F and cobalt ferrite (F).

As follows from Figure 4a, isotherms of N<sub>2</sub> adsorption-desorption were S-shaped, with a characteristic hysteresis loop typical of IV-type isotherms in the IUPAC classification [59]. The presence of hysteresis in the isotherms is evidence for mesopores in these materials [60] that, in the case of layered aluminosilicates, is caused by the secondary porosity in gaps between the particles [61]. The shape of hysteresis is strongly differed for samples of cobalt ferrite and bentonite that testified to a difference in the surface morphology and pore shape

of the investigated samples. The presence of slit-like pores (H3 type of hysteresis [60]) as well as ink-bottle-like pores [62] is characteristic for clay minerals. Unlike the samples containing Bt, the branch of N<sub>2</sub> desorption at the isotherm of CoFe<sub>2</sub>O<sub>4</sub> lay quite close to the adsorption branch, thus, showing the low volume of slit-like mesopores. In addition, the shape of the isotherm obtained for cobalt ferrite was similar to type III which may indicate the practical absence of micropores and the presence of a certain amount of large mesopores with  $D > 50$  nm (or the so called “small macropores”). The highest adsorption volume of nitrogen was found for the sample of the natural clay material Bt, while the lowest one was for the sample of pure CoFe<sub>2</sub>O<sub>4</sub>, adsorption capacity of which was mainly due to the outer surface of nanosized particles and gaps between them. The addition and increasing of the content of cobalt ferrite phase from 10 to 20 mass % in the composite material led to an ever deeper decline of the N<sub>2</sub> adsorption volume that illustrated the transformations of the material porosity and, hence, the change in the value of the specific surface area.

The pore size distributions (Figure 4b) testified to their polymodal nature for all the samples studied, consisting in the presence of mostly mesopores in the ranges of 3–10 nm, 20–50 nm and 65–75 nm. The character of the porosity of composite samples Bt-10F and Bt-20F changed as a result of meso- and micropores [1] obstruction by the CoFe<sub>2</sub>O<sub>4</sub> nanoparticles of appropriate size (Figure 3b). As a consequence, the fraction of pores with a diameter of about 40 nm declined, while the fraction of pores of 45–50 nm in size rose. The contribution of large mesopores (65–75 nm) increased for the Bt-10F sample and then decreased for Bt-20F, pointing out their filling with ferrite nanoparticles.

Table 2 introduces values for the specific surface area and the porosity of investigated samples. The introduction of 10–20 mass % of cobalt ferrite into the composition resulted in the 30%–36% decline of the specific surface area of the resulting composite material as compared to the Bt sample. This was due to the contraction of the mesopore volume and the absence of the micropores contribution to nitrogen sorption. Such tendency is consistent with the data of [1], indicating a decrease of the microporosity of zeolite by its modification with CoFe<sub>2</sub>O<sub>4</sub> to produce a faujasite-CoFe<sub>2</sub>O<sub>4</sub> composite. The volume of macropores for the Bt-10F and Bt-20F samples slightly increased in regard to that of Bt, whereas the average pore diameter decreased a bit.

**Table 2.** Specific surface area and porosity of Bt, CoFe<sub>2</sub>O<sub>4</sub> and composites on their base.

Sample	S <sub>BET</sub> , m <sup>2</sup> /g	Pore Volume, cm <sup>3</sup> /g				Pore Diameter, D, nm
		V <sub>micro</sub>	V <sub>meso</sub>	V <sub>macro</sub> * 50–75 nm	V <sub>total</sub>	
Bt	85	0.0368	5.4862	2.1076	7.6306	7.0
Bt-10F	60	0	4.6870	2.2472	6.9342	4.9
Bt-20F	54	0	4.4298	2.2176	6.6474	6.6
F	16	0	1.7951	1.2553	3.0504	21.4

\* Determined from experimental data on cumulative pore volume (Reports S1–S4).

The observed changes in the surface morphology of the composite material samples based on natural bentonite and cobalt ferrite may result in both an increase in its adsorption capacity and its weakening, that is determined by the type of the sorbate and by the mechanism of the sorption process.

As an example of another sorbate, the properties and industrial application of which may define the area of use of the new composite material, one considers hereinafter aqueous solutions of formaldehyde: an industrial toxicant often found in wastewaters and emissions of paint varnish, furniture, chemical and other manufactories. Table 3 illustrates the values of adsorption of formaldehyde from aqueous solutions by investigated samples. Previous studies [47] revealed the possibility of formaldehyde sorption from aqueous media by a composite doped with 20 mass % of spinel.

**Table 3.** Adsorption capacity (mg/g) of bentonite, cobalt ferrite and composites on their base towards formaldehyde in aqueous solutions of various concentrations (20 °C).

Sample	Concentration of Equilibrium Solution			
	0.038 M	0.102 M	0.201 M	0.388 M
Bt	3.15	14.2	20.8	27.0
Bt-10F	4.0	14.8	21.5	28.6
Bt-20F	4.1	15.6	22.6	30.0
F	4.2	10.5	11.2	13.2

As follows from Table 3, the increase in the concentration of equilibrium solution caused the rise of adsorption capacity of each sorbent. At the same time, in the region of low concentrations (0.038 M), the adsorption of formaldehyde by the sample of cobalt ferrite, as well as by the Bt-10F and Bt-20F composites, was 27%–33% higher than that for the Bt sample. In the region of higher concentrations (0.102–0.388 M), the adsorption behavior of the samples changed: the sample F manifested its saturation (the isotherm reached a plateau [47]) and, as a result, had lower values of the adsorption capacity (in 1.5–2.3 times) as compared to the samples Bt, Bt-10F and Bt-20F. Taking into account that on the surface of copper ferrite ( $\text{CuFe}_2\text{O}_4$ ) the process of formaldehyde chemisorption (with an energy of  $-107.15$  kJ/mol) occurred [63], as well as a change in the adsorption mechanism from physical adsorption through ion-exchange to chemical adsorption with an increase in the transition metal content in the ferrite phase [64], we also tend to conclude that the primary contribution of the chemisorption mechanism during the uptake of formaldehyde by a sample of cobalt ferrite was probably due to the interaction of  $\text{Fe}^{3+}$  and  $\text{Co}^{2+}$  ions of ferrite surface with hydroxyl groups of formaldehyde hydrate present in the solution.

Unlike the ferrite sample, the sorption process at the surface of aluminosilicate Bt and composite Bt-10F, Bt-20F samples exhibited a distinct polymolecular character in the concentration range above  $0.1 \text{ mol/dm}^3$ . This fact was also discovered in [65] by the sorption of formaldehyde on zeolites, activated carbon, mesoporous silica and MOF MIL-53. The presence of different species in aqueous formaldehyde solutions, e.g., products of the interaction of formaldehyde with water molecules forming methylene glycol  $\text{HO-CH}_2\text{-OH}$ , products of formaldehyde polymerization (paraformaldehyde,  $n = 8\text{--}100$ ), as well as products of formaldehyde reaction with methanol [66], 10% of which is being usually added to formalin for its stabilization, contributes to this process. The developed morphology of the surface of the samples Bt, composite sorbents Bt-10F and Bt-20F promotes a greater sorption of formaldehyde in comparison with the ferrite sample. In addition, despite a 1.4–1.6-fold decrease in the specific surface area of the Bt sample by its modification with ferrite, its sorption capacity did not decrease, but increased by  $\sim 6\text{--}12\%$  (in the order  $\text{Bt} > \text{Bt-10F} > \text{Bt-20F}$  in 0.388 M solution). This fact, from the one side, can be caused by the change and the redistribution of the surface active sites ratio (hydroxyl groups  $\text{Si-OH}$ ,  $\text{Si-OH-Al}$ ,  $\text{Al-OH}$ ,  $\text{Fe-OH}$ , coordinately unsaturated cations  $\text{Al}^{3+}$  and  $\text{Si}^{4+}$  and hydrated exchangeable cations  $\text{Ca}^{2+}$  and  $\text{Na}^+$ ) by the bentonite modification with ferrite; from the other side, it confirmed the decisive contribution of polymolecular sorption to the uptake of formaldehyde from aqueous solutions by materials based on aluminosilicates [65,67]. The latter fact is supported by the distinct changes in the IR spectrum of the Bt-10F composite material after formaldehyde adsorption (Figure 2d and Figures S3 and S4 of Supplementary Materials). The broadening of the band of deformation vibrations of water at  $1635 \text{ cm}^{-1}$  and a strong increase in the intensity and width of the band of stretching vibrations of  $\text{-O-H}$  bonds in the region of  $3200\text{--}3500 \text{ cm}^{-1}$  may be associated with the predominant sorption of formaldehyde hydrate molecules, its associates, as well as its oligomers, through the formation of hydrogen bonds with the surface sites of the composite sorbent. Nevertheless, the value of adsorption capacity towards formaldehyde for the obtained composite materials did not exceed those for the case of clay minerals' modification with acid and alkali solutions [47,68].

### 3.3. Magnetic Properties of Bentonite, $\text{CoFe}_2\text{O}_4$ Spinel and Composites on Their Base

The investigated natural clay material is a paramagnet with a specific magnetic susceptibility  $\chi_g = 9.1 \times 10^{-6}$  emu/g at  $T = 298$  K, which gives an effective magnetic moment of  $3.62 \mu\text{B}$  per iron atom. This value is significantly lower than that of  $\text{Fe}^{3+}$  ( $5.9 \mu\text{B}$ ) or  $\text{Fe}^{2+}$  ( $\sim 5.2 \mu\text{B}$ ) [69], which may indicate the existence of antiferromagnetic interactions in the bentonite sample or the presence of a part of iron in an antiferromagnetic oxide phase.

Figure 5 illustrates the occurrence of the magnetic susceptibility in the Bt-10F and Bt-20F samples of the composite as compared to the bentonite sample.

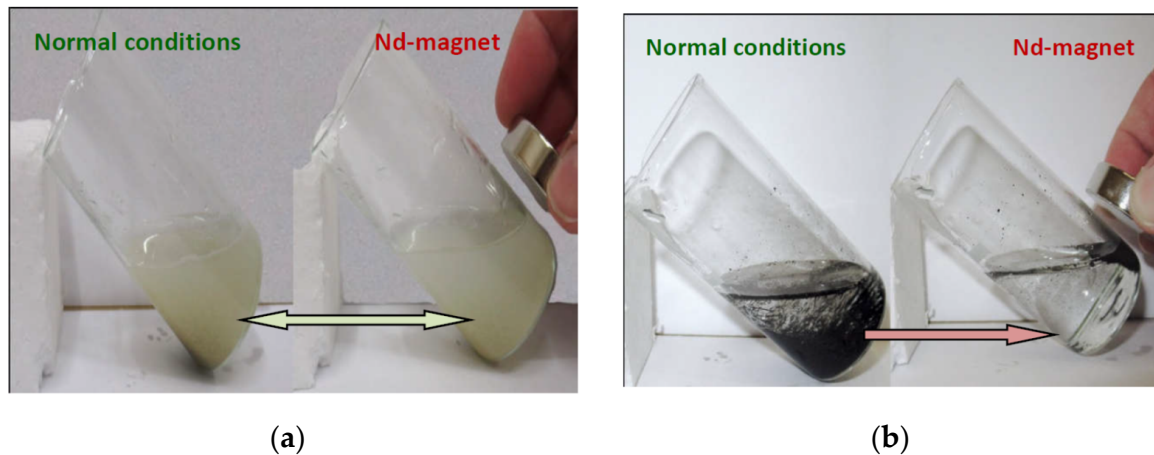


**Figure 5.** Suspensions of the investigated sorbents in an equilibrium formaldehyde solution in the presence and absence of an external magnetic field (Nd magnet): (a) suspension of Bt sample; (b) suspension of Bt-10F composite sample.

As it follows from Figure 5a, the suspension of Bt in an aqueous formaldehyde solution did not separate under action of the Nd magnet due to the paramagnetic nature of clay minerals. The material acquired magnetism when it was doped by the  $\text{CoFe}_2\text{O}_4$  phase forming composite samples Bt-10F and Bt-20F, as confirmed by Figure 5b. Suspensions of the composite sorbents Bt-10F and Bt-20F were easily separable from the equilibrium solution by the action of the external magnetic field owing to the presence of magnetic elements Co and Fe in the composite phase.

Figure 6 shows the dependence of the magnetization on the external magnetic field for ferrite, bentonite and composite Bt-20F samples.

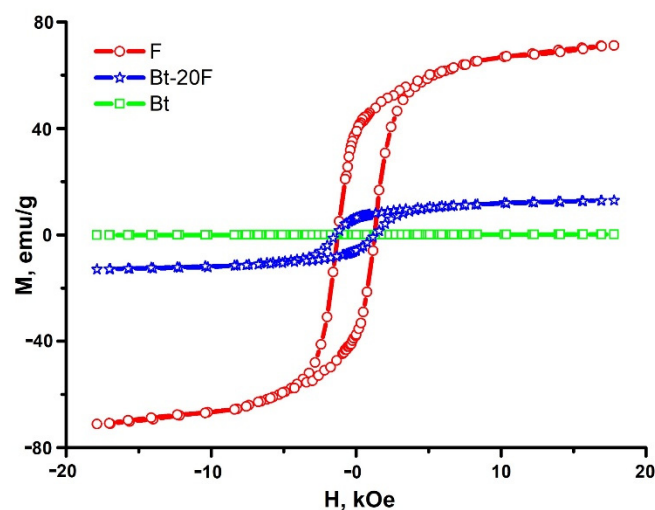


**Figure 6.** Magnetic properties of bentonite (Bt), cobalt ferrite (F) and composite (Bt-20F).

The samples F and Bt-20F demonstrated the dependence of magnetization on the field, which is typical for hard magnetic materials [57,70]. The coercive force for the sample F was 1290 Oe and 1360 Oe for the sample Bt-20F. The saturation magnetization of F was 71.1 emu/g. For the Bt-20F composite, the saturation magnetization was 12.9 emu/g. The values of the coercive force and saturation magnetization of the Bt-20F composite satisfied the solution of the problem of its extraction from an aqueous suspension under the action of an external magnetic field at ambient temperature. This allowed us to consider the proposed sorbent as magnetically sensitive and magnetically controllable.

#### 4. Conclusions

The new nanosorbent combining two functional properties, sorption and magnetic ones, was formed based on the layered aluminosilicate and nanodispersed ferromagnetic spinel  $\text{CoFe}_2\text{O}_4$ . The magnetic sorbent was formed by activating natural ferruginous nanoporous aluminosilicate via doping it with a finely dispersed  $\text{CoFe}_2\text{O}_4$  spinel. According to the obtained data of XRD, FTIR spectroscopy and TEM, spinel nanoparticles are statistically distributed in the volume of the aluminosilicate phase, thereby leveling the contribution of micropores completely, significantly reducing the volume of mesopores and the specific surface area of the sorbent by 29%–35%. At the same time, the paradox of retaining the sorption activity of the nanocomposite with respect to the industrial toxicant formaldehyde was revealed. Nano inclusions of the spinel are assumed to act as a chemical activator of the sorbent surface, modifying and imparting it new properties. Obviously, the increase in the chemo-activity of the magnetic nanocomposite pores, along with the features of the sorbate molecule prone to intermolecular interactions and polymerization, resulted in the phenomenon of the polymolecular sorption and retaining the sorbent capacity. Owing to its magnetic properties, the new nanocomposite sorbent has the advantage of selective separation from the aqueous medium by an external magnetic field and has the solid application potential in sorption technologies of recycling and environment protecting means. The regeneration of the aluminosilicate sorbent is successfully feasible applying electrolyte solutions, leading to sorbate desorption or chemical binding in the case of  $\text{NH}_4^+$ -ions. by treating it with a green oxidant  $\text{H}_2\text{O}_2$ . This is the focus of our further investigations.

**Supplementary Materials:** The following supporting information can be downloaded at: <https://www.mdpi.com/article/10.3390/min12111474/s1>. Figure S1: XRD patterns of investigated samples of Bt,  $\text{CoFe}_2\text{O}_4$  and composites Bt-10F, Bt-20F, Phase designations: Sm—smectite, I—illite, K—kaolinite, Q—quartz, Fs—feldspars; Figure S2: FTIR spectrum of Bt; Figure S3: FTIR spectrum of Bt-10F; Figure S4: FTIR spectrum of Bt-10F+sorb after adsorption of formaldehyde; Table S1: Chemical composition of the samples; Report S1: BET data Bt; Report S2: BET data Bt-10F; Report S3: BET data Bt-20F; Report S4: BET data\_  $\text{CoFe}_2\text{O}_4$ .

**Author Contributions:** Conceptualization, N.K. (Nataliya Khodosova), L.N., E.T. (Elena Tomina) and L.B.; Methodology, E.T. (Elena Tomina), N.K. (Nataliya Khodosova), L.N., V.K., E.T. (Ekaterina Tyupina), A.V. and P.K.; validation, E.T. (Elena Tomina), N.K. (Nataliya Khodosova), L.N., V.K., E.T. (Ekaterina Tyupina) and A.V.; investigation, N.K. (Nikolay Kurkin), O.Z., T.K., N.K. (Nataliya Khodosova), L.N. and A.V.; resources, E.T. (Elena Tomina), L.B.; V.K., A.Z. and P.K.; data curation, L.N., N.K. (Nataliya Khodosova) and V.K.; writing—original draft preparation, N.K. (Nataliya Khodosova), L.N., A.V., O.Z. and T.K.; writing—review and editing, N.K. (Nataliya Khodosova), L.N., E.T. (Elena Tomina), L.B., V.K., A.V., P.K. and E.T. (Ekaterina Tyupina); visualization, N.K. (Nataliya Khodosova), L.N., V.K., O.Z., T.K. and E.T. (Elena Tomina); supervision, E.T. (Elena Tomina); project administration, L.N. and N.K. (Nataliya Khodosova); funding acquisition, E.T. (Elena Tomina) and V.K. All authors have read and agreed to the published version of the manuscript.

**Funding:** This research was partially supported by Voronezh State Forest Engineering University named after G.F. Morozov. Methodological developments for the detailed identification of the smectite transformation due to various treatments were carried out as part of the RSF project #22-17-00252. The APC was funded partially by the Voronezh State University of Forestry and Technologies named after G.F. Morozov.

**Data Availability Statement:** The data presented in this study are available in the article and in the supplementary material.

**Acknowledgments:** The equipment of the Center for Collective Use of the Voronezh State University, <http://ckp.vsu.ru> (accessed on 18 November 2022) (X-ray fluorescence spectrometer S8 Tiger, Bruker AXS GmbH, IR-Fourier spectrometer Vertex-70, Bruker, transmission electron microscope CarlZeiss Libra-120, scanning electron microscope JSM-6380LV JEOL) and the equipment, acquired at the expense of the Development Program of Moscow State University named after M.V. Lomonosov (X-ray diffractometer Ultima-IV, Rigaku) was used. The authors would like to acknowledge Marina Alekhina, Mendeleev University of Chemical Technology, and Alexander Dmitrenkov, Voronezh State University of Forestry and Technologies, for their assistance in organizing the studies of magnetic properties of the materials.

**Conflicts of Interest:** The authors declare no conflict of interest.

## References

1. Paris, E.; Malafatti, J.; Musetti, H.; Manzoli, A.; Zenatti, A.; Escote, M. Faujasite zeolite decorated with cobalt ferrite nanoparticles for improving removal and reuse in  $Pb^{2+}$  ions adsorption. *Chin. J. Chem. Eng.* **2020**, *28*, 1884–1890. [CrossRef]
2. Suppaso, C.; Pongkan, N.; Intachai, S.; Ogawa, M.; Khaorapapong, N. Magnetically recoverable  $\beta$ -Ni(OH)<sub>2</sub>/ $\gamma$ -Fe<sub>2</sub>O<sub>3</sub>/NiFe-LDH composites; isotherm, thermodynamic and kinetic studies of synthetic dye adsorption and photocatalytic activity. *Appl. Clay Sci.* **2021**, *213*, 106115. [CrossRef]
3. Agboola, O.; Popoola, P.; Sadiku, R.; Sanni, S.E.; Fayomi, S.O.; Fatoba, O.S. Nanotechnology in Wastewater and the Capacity of Nanotechnology for Sustainability. In *Environmental Nanotechnology Volume 3. Environmental Chemistry for a Sustainable World*; Dasgupta, N., Ranjan, S., Lichtfouse, E., Eds.; Springer: Cham, Switzerland, 2020; Volume 27, pp. 1–45.
4. Sahu, J.; Karri, R.R.; Zabed, H.M.; Shams, S.; Qi, X. Current perspectives and future prospects of nano-biotechnology in wastewater treatment. *Sep. Purif. Rev.* **2021**, *50*, 139–158. [CrossRef]
5. Guo, W.; Fu, Z.; Zhang, Z.; Wang, H.; Liu, S.; Feng, W.; Zhao, X.; Giesy, J.P. Synthesis of Fe<sub>3</sub>O<sub>4</sub> magnetic nanoparticles coated with cationic surfactants and their applications in Sb (V) removal from water. *Sci. Total Environ.* **2020**, *710*, 136302. [CrossRef]
6. Rashid, R.; Shafiq, I.; Akhter, P.; Iqbal, M.J.; Hussain, M. A state-of-the-art review on wastewater treatment techniques: The effectiveness of adsorption method. *Environ. Sci. Pollut. Res.* **2021**, *28*, 9050–9066. [CrossRef]
7. Dethe, M.J.; Marathe, K.V.; Gaikar, V.G. Adsorption of Lactic Acid on Weak Base Polymeric Resins. *Sep. Sci. Technol.* **2006**, *41*, 2947–2971. [CrossRef]
8. Hall, S.; Tang, R.; Baeyens, J.; Dewil, R. Removing polycyclic aromatic hydrocarbons from water by adsorption on silicagel. *Polycycl. Aromat. Compd.* **2009**, *29*, 160–183. [CrossRef]
9. Koster, H.M.; Ehrlicher, U.; Gilg, H.; Jordan, R.; Murad, E.; Onnich, K. Mineralogical and chemical characteristics of five nontronites and Fe-rich smectite. *Clay Miner.* **1999**, *34*, 579–599. [CrossRef]
10. Azam, K.; Raza, R.; Shezad, N.; Shabir, M.; Yang, W.; Ahmad, N.; Shafiq, I.; Akhter, P.; Razzaq, A.; Hussain, M. Development of recoverable magnetic mesoporous carbon adsorbent for removal of methyl blue and methyl orange from wastewater. *J. Environ. Chem. Eng.* **2020**, *8*, 104220. [CrossRef]
11. Abidi, N.; Errais, E.; Duplay, J.; Berez, A.; Jrad, A.; Schäfer, G.; Ghazi, M.; Semhi, K.; Trabelsi-Ayadi, M. Treatment of dye-containing effluent by natural clay. *J. Clean. Prod.* **2015**, *86*, 432–440. [CrossRef]
12. Juang, R.-S.; Lin, S.-H.; Tsao, K.-H. Mechanism of the Sorption of Phenols from Aqueous Solutions into Surfactant-Modified Montmorillonite. *J. Colloid Interface Sci.* **2002**, *254*, 234–241. [CrossRef] [PubMed]
13. Bel'chinskaya, L.I.; Khodosova, N.A.; Novikova, L.A.; Anisimov, M.V.; Petukhova, G.A. Regulation of sorption processes in natural nanoporous aluminosilicates. 3. Impact of electromagnetic fields on adsorption and desorption of formaldehyde by clinoptilolite. *Prot. Met. Phys. Chem. Surf.* **2017**, *53*, 793–800. [CrossRef]
14. Bel'chinskaya, L.I.; Khodosova, N.A.; Novikova, L.A.; Strel'nikova, O.Y.; Roessner, F.; Petukhova, G.A.; Zhabin, A.V. Regulation of sorption processes in natural nanoporous aluminosilicates. 2. Determination of the ratio between active sites. *Prot. Met. Phys. Chem. Surf.* **2016**, *52*, 599–606. [CrossRef]
15. Gubin, S.P.; Koksharov, Y.A.; Khomutov, G.B.; Yurkov, G.Y. Magnetic nanoparticles: Preparation, structure and properties. *Russ. Chem. Rev.* **2005**, *74*, 539–574. [CrossRef]
16. Lu, A.-H.; Salabas, E.L.; Schuth, F. Magnetic nanoparticles: Synthesis, protection, functionalization, and application. *Angew. Chem. Int. Ed.* **2007**, *46*, 1222–1244. [CrossRef]
17. Soltani, N.; Salavati, H.; Moghadasi, A. The role of Na-montmorillonite/cobalt ferrite nanoparticles in the corrosion of epoxy coated AA 3105 aluminum alloy. *Surf. Interfaces* **2019**, *15*, 89–99. [CrossRef]
18. Aguiara, A.S.; Michels, L.; da Silva, F.G.; Kernc, C.; Gomide, G.; Ferreira, C.M.; Depuyrot, J.; Aquino, R.; da Silva, G.J. The use of a laponite dispersion to increase the hydrophilicity of cobalt ferrite magnetic nanoparticles. *Appl. Clay Sci.* **2020**, *193*, 105663. [CrossRef]

19. Mahmoud, M.E.; Abdelwahab, M.S.; Fathallah, E.M. Design of novel nano-sorbents based on nano-magnetic iron oxide-bound-nano-silicon oxide-immobilized-triethylenetetramine for implementation in water treatment of heavy metals. *Chem. Eng. J.* **2013**, *223*, 318–327. [CrossRef]
20. Haicheng, L.; Wei, C.; Cheng, L.; Yu, L.; Changlong, D. Magnetic mesoporous clay adsorbent: Preparation, characterization and adsorption capacity for atrazine. *Microporous Mesoporous Mater.* **2014**, *194*, 72–78.
21. Lutfullin, M.A.; Shornikova, O.N.; Vasiliev, A.V.; Pokholok, K.V.; Osadchaya, V.A.; Saidaminov, M.I.; Sorokina, N.E.; Avdeev, V.V. Petroleum products and water sorption by expanded graphite enhanced with magnetic iron phases. *Carbon* **2014**, *66*, 417–425. [CrossRef]
22. Tkachenko, I.A.; Panasenko, A.E.; Odinokov, M.M.; Marchenko, Y.V. Magnetoactive Composite Sorbents  $\text{CoFe}_2\text{O}_4\text{-SiO}_2$ . *Russ. J. Inorg. Chem.* **2020**, *65*, 1142–1149. [CrossRef]
23. Tolmacheva, V.V.; Apyari, V.V.; Kochuk, E.V.; Dmitrenko, S.G. Magnetic adsorbents based on iron oxide nanoparticles for the extraction and preconcentration of organic compounds. *J. Anal. Chem.* **2016**, *71*, 339–356. [CrossRef]
24. Germanov, E.P.; Kutushev, M.V. Magnetically Controlled Sorbent and a Method for Manufacture Thereof (Russia, Patent RU 2 255 800 C1) Rospatent. 2003. Available online: <https://rospatent.gov.ru> (accessed on 10 July 2005).
25. Kharisov, B.I.; Dias, V.R.; Kharissova, O.V. Mini-review: Ferrite nanoparticles in the catalysis. *Arab. J. Chem.* **2014**, *104*, 1–7. [CrossRef]
26. Akbarzadeh, A.; Samiei, M.; Davaran, S. Magnetic nanoparticles: Preparation, physical properties, and applications in biomedicine. *Nanoscale Res. Lett.* **2012**, *7*, 144–156. [CrossRef]
27. Agafonov, A.V.; Grishina, E.P. Nanocomposites of Inorganic Oxides with Ionic Liquids. Synthesis, Properties, Application (Review). *Russ. J. Inorg. Chem.* **2019**, *64*, 1641–1648. [CrossRef]
28. Ali, I.; AlOthman, Z.A.; Sanagi, M.M. Green Synthesis of iron nano-impregnated adsorbent for fast removal of fluoride from Water. *J. Mol. Liq.* **2015**, *211*, 457–465. [CrossRef]
29. Cui, L.; Wang, Y.; Gao, L.; Hu, L.; Yan, L.; Wei, Q.; Du, B. EDTA functionalized magnetic graphene oxide for removal of Pb(II), Hg(II) and Cu(II) in water treatment: Adsorption mechanism and separation property. *Chem. Eng. J.* **2015**, *28*, 1–10. [CrossRef]
30. Ali, I.; AlOthman, Z.A.; Al-Warthan, A. Synthesis of composite iron nano adsorbent and removal of ibuprofen drug residue from water. *J. Mol. Liq.* **2016**, *219*, 858–864. [CrossRef]
31. Roshanfekr Rad, L.; Anbia, M. Zeolite-based composites for the adsorption of toxic matters from water: A review. *J. Environ. Chem. Eng.* **2021**, *9*, 106088. [CrossRef]
32. Zhang, J.; Khan, M.A.; Xia, M.; Abdo, A.M.; Lei, W.; Liao, C.; Wang, F. Facile hydrothermal synthesis of magnetic adsorbent  $\text{CoFe}_2\text{O}_4/\text{MMT}$  to eliminate antibiotics in aqueous phase: Tetracycline and ciprofloxacin. *Environ. Sci. Pollut. Res.* **2019**, *26*, 215–226. [CrossRef]
33. Vidal, C.B.; Santos, B.A.; França, A.M.; Bessa, R.A.; Loiola, A.R.; Nascimento, R.F. Magnetite-Zeolite Nanocomposite Applied to Remediation of Polluted Aquatic Environments. In *Nanomaterials and Nanotechnology*; Nascimento, R.F., Sousa Neto, V.O., Almeida Fehine, P.B., Cavalcante Freire, P.T., Eds.; Springer: Singapore, 2021; pp. 69–94.
34. Reddy, D.H.K.; Yun, Y.-S. Spinel ferrite magnetic adsorbents: Alternative future materials for water purification? *Coord. Chem. Rev.* **2016**, *315*, 90–111. [CrossRef]
35. Shapkin, N.P.; Khal'chenko, I.G.; Pechnikov, V.S.; Mayorov, V.Y.; Maslova, N.V.; Razov, V.I.; Papynov, E.K. Magnetic Composites Based on Cobalt Ferrite, Vermiculite, and Rice Husks: Synthesis and Properties. *Russ. J. Inorg. Chem.* **2020**, *65*, 1614–1622. [CrossRef]
36. Salunkhe, A.B.; Khot, V.M.; Thorat, N.D.; Phadatare, M.R.; Sathish, C.I.; Dhawale, D.S.; Pawar, S.H. Polyvinyl alcohol functionalized cobalt ferrite nanoparticles for biomedical applications. *Appl. Surf. Sci.* **2013**, *264*, 598–604. [CrossRef]
37. Liu, F.; Laurent, S.; Fattahi, H.; Vander Elst, L.; Muller, R.N. Superparamagnetic nanosystems based on iron oxide nanoparticles for biomedical imaging. *Nanomedicine* **2011**, *6*, 519–528. [CrossRef] [PubMed]
38. Petrova, E.; Kotsikau, D.; Pankov, V.; Fahmi, A. Influence of Synthesis Methods on Structural and Magnetic Characteristics of Mg–Zn-Ferrite Nanopowders. *J. Magn. Magn. Mater.* **2019**, *473*, 85–91. [CrossRef]
39. Somnath, S.; Indu, S.; Kotnala, R.K.; Singh, M.; Kumar, A.; Dhiman, P.; Singh, V.P.; Verma, K.; Kumar, G. Structural Magnetic and Mössbauer Studies of Nd-Doped Mg-Mn Ferrite Nanoparticles. *J. Magn. Magn. Mater.* **2017**, *444*, 77–86. [CrossRef]
40. Manikandan, A.; Sridhar, R.; Antony, S.A.; Ramakrishna, S. A Simple Aloe Vera Plant-Extracted Microwave and Conventional Combustion Synthesis: Morphological, Optical, Magnetic and Catalytic Properties of  $\text{CoFe}_2\text{O}_4$  Nanostructures. *J. Mol. Struct.* **2014**, *1076*, 188–200. [CrossRef]
41. Song, Q.; Zhang, Z.J. Shape Control and Associated Magnetic Properties of Spinel Cobalt Ferrite Nanocrystals. *J. Am. Chem. Soc.* **2004**, *126*, 6164–6168. [CrossRef]
42. Pallai, V.; Shah, D.O. Synthesis of High-Coercivity Cobalt Ferrite Particles Using Water-in-Oil Microemulsions. *J. Magn. Magn. Mater.* **1996**, *163*, 243–248. [CrossRef]
43. Skomski, R. Nanomagnetism. *J. Phys. Condens. Matter.* **2003**, *15*, 841–896. [CrossRef]
44. Chen, L.; Zhou, C.H.; Fiore, S.; Tong, D.S.; Zhang, H.; Li, C.S.; Ji, S.F.; Yu, W.H. Functional magnetic nanoparticle/clay mineral nanocomposites: Preparation, magnetism and versatile applications. *Appl. Clay Sci.* **2016**, *127–128*, 143–163. [CrossRef]
45. Zhang, S.; Zhong, L.; Yang, H.; Tang, A.; Zuo, X. Magnetic carbon-coated palygorskite loaded with cobalt nanoparticles for Congo Red removal from waters. *Appl. Clay Sci.* **2020**, *198*, 105856. [CrossRef]

46. Palza, H.; Delgado, K.; Govan, J. Novel magnetic  $\text{CoFe}_2\text{O}_4$ /layered double hydroxide nanocomposites for recoverable anionic adsorbents for water treatment. *Appl. Clay Sci.* **2019**, *183*, 105350. [[CrossRef](#)]
47. Khodosova, N.A.; Tomina, E.V.; Belchinskaya, L.I.; Zhabin, A.V.; Volkov, A.S.; Kurkin, N.A. Physical and Chemical Characteristics Of A Nanocomposite Sorbent, Nontronite/ $\text{CoFe}_2\text{O}_4$ . *J. Sorp. Chromatogr. Proces.* **2021**, *24*, 520–528.
48. Bartenev, V.K.; Savko, A.D. Lithology, facies and minerals of the Paleogene of the TsChER. In *Proceedings of the Scientific Research Institute of Geology of the Voronezh State University*; SINOAL: Voronezh, Russia, 2001; Volume 7, 146p.
49. Shashank, D.B.; Rakesh, K.S.; Vivek, K.; Nishant, K.; Shambhu, K. Tailoring the structural, optical and multiferroic properties of low temperature synthesized cobalt ferrite nanomaterials, by citrate precursor method. *Mater. Today Proc.* **2021**, *46*, 6527–6533.
50. Ali, T.M.; Ismail, S.M.; Mansour, S.F.; Abdo, M.A.; Yehia, M. Physical properties of Al-doped cobalt nanoferrite prepared by citrate–nitrate auto combustion method. *J. Mater. Sci. Mater. Electron.* **2021**, *32*, 3092–3103. [[CrossRef](#)]
51. Mariosi, F.R.; Venturini, J.; Alexandre, C.V.; Bergmann, C.P. Lanthanum-doped spinel cobalt ferrite ( $\text{CoFe}_2\text{O}_4$ ) nanoparticles for environmental applications. *Ceram. Int.* **2019**, *46*, 2772–2779. [[CrossRef](#)]
52. JCPDC PCPDFWIN: A Windows Retrieval/Display Program for Accessing the ICDD PDF—2 Data Base; International Centre for Diffraction Data: Newtown Square, PA, USA, 1997.
53. Subasi, N.T. Formaldehyde Advantages and Disadvantages: Usage Areas and Harmful Effects on Human Beings. In *Bio-Chemical Toxicology—Heavy Metals and Nanomaterials*; Ince, M., Ince, O.K., Ondrasek, G., Eds.; IntechOpen: London, UK, 2020.
54. Gates, W.P. Infrared spectroscopy and the chemistry of dioctahedral smectites. In *Vibrational Spectroscopy of Layer Silicates and Hydroxides*, 1st ed.; Kloppege, J.T., Ed.; The Clay Mineral Society: Aurora, CO, USA, 2005; pp. 126–168.
55. Rojas-Mantilla, H.D.; Ayala-Duran, S.C.; Pupo Nogueira, R.F. Nontronite mineral clay NAu-2 as support for hematite applied as catalyst for heterogeneous photo-Fenton processes. *Chemosphere* **2021**, *277*, 130258. [[CrossRef](#)]
56. Madejova, J.; Komadel, P. Baseline Studies Of The Clay Minerals Society Source Clays: Infrared Methods. *Clays Clay Miner.* **2001**, *49*, 410–432. [[CrossRef](#)]
57. Figgis, B.N.; Lewis, J. The Magnetochemistry of Complex Compounds. In *Modern Coordination Chemistry*; Lewis, J., Wilkins, R.G., Eds.; Wiley: New York, NY, USA, 1960.
58. Krupskaya, V.; Novikova, L.; Tyupina, E.; Belousov, P.; Dorzhieva, O.; Zakusin, S.; Kim, K.; Roessner, F.; Badetti, E.; Brunelli, A.; et al. The influence of acid modification on the structure of montmorillonites and surface properties of bentonites. *Appl. Clay Sci.* **2019**, *172*, 1–10. [[CrossRef](#)]
59. Donohue, M.D.; Aranovich, G.L. Classification of Gibbs adsorption isotherms. *Adv. Colloid Interface Sci.* **1998**, *76–77*, 137–152. [[CrossRef](#)]
60. Horikawa, T.; Do, D.D.; Nicholson, D. Capillary condensation of adsorbates in porous materials. *Adv. Colloid Interface Sci.* **2011**, *169*, 40–58. [[CrossRef](#)] [[PubMed](#)]
61. Asaad, A.; Hubert, F.; Ferrage, E.; Dabat, T.; Paineau, E.; Porion, P.; Savoye, S.; Gregoire, B.; Dazas, B.; Delville, A.; et al. Role of interlayer porosity and particle organization in the diffusion of water in swelling clays. *Appl. Clay Sci.* **2021**, *207*, 106089. [[CrossRef](#)]
62. Wang, X.; Cheng, H.; Chai, P.; Bian, J.; Wang, X.; Liu, Y.; Yin, X.; Pan, S.; Pan, Z.H. Pore Characterization of Different Clay Minerals and Its Impact on Methane Adsorption Capacity. *Energy Fuels.* **2020**, *34*, 12204–12214. [[CrossRef](#)]
63. Ding, J.; Yang, Y.; Liu, J.; Liu, F.; Yu, Y. Experimental and theoretical studies on formaldehyde catalytic combustion over Cu–Fe spinel-type catalyst. *Proc. Combust. Inst.* **2021**, *38*, 6483–6491. [[CrossRef](#)]
64. Tatarchuk, T.; Myslin, M.; Mironyuk, I.; Bououdina, M.; Pedziwiatr, A.T.; Gargula, R.; Bogacz, B.F.; Kurzydło, P. Synthesis, morphology, crystallite size and adsorption properties of nanostructured Mg–Zn ferrites with enhanced porous structure. *J. Alloys Compd.* **2020**, *819*, 152945. [[CrossRef](#)]
65. Bellat, J.P.; Bezverkhyy, I.; Weber, G.; Royer, S.; Averlant, R.; Giraudon, J.M.; Lamonier, J.F. Capture of formaldehyde by adsorption on nanoporous materials. *J. Hazard. Mater.* **2015**, *300*, 711–717. [[CrossRef](#)]
66. Detcheberry, M.; Destrac, P.; Meyer, X.M.; Condoret, J.-S. Phase equilibria of aqueous solutions of formaldehyde and methanol: Improved approach using UNI-QUAC coupled to chemical equilibria. *Fluid Phase Equilib.* **2015**, *392*, 84–94. [[CrossRef](#)]
67. Novikova, L.A.; Bogdanov, D.S.; Belchinskaya, L.I.; Kolousek, D.; Doushova, B.; Lhotka, M.; Petukhova, G.A. Adsorption of Formaldehyde from Aqueous Solutions Using Metakaolin-Based Geopolymer Sorbents. *Prot. Met. Phys. Chem. Surf.* **2019**, *55*, 864–871. [[CrossRef](#)]
68. Bel'chinskaya, L.I.; Khodosova, N.A.; Strel'nikova, O.Y.; Petukhova, G.A.; Ciganda, L. Regulation of Sorption Processes on Natural Nanoporous Aluminosilicates. 1. Acidic and Basic Modifications. *Prot. Met. Phys. Chem. Surf.* **2015**, *51*, 779–786. [[CrossRef](#)]
69. Kurian, M.; Thankachan, S.; Nair, D.S.; Aswathy, E.K.; Aswathy, B.; Arathy, T.; Binu Krishna, K.T. Structural, magnetic, and acidic properties of cobalt ferrite nanoparticles synthesised by wet chemical methods. *J. Adv. Ceram.* **2015**, *4*, 199–205. [[CrossRef](#)]
70. Fedotova, J.A.; Baev, V.G.; Lesnikovich, A.I.; Milevich, A.I.; Vorobjova, S.A. Magnetic properties and local configurations of 57Fe atoms in  $\text{CoFe}_2\text{O}_4$  powders and  $\text{CoFe}_2\text{O}_4$ /PVA nanocomposites. *Phys. Solid Stat.* **2011**, *53*, 694–700. [[CrossRef](#)]